



Fermi National Accelerator Laboratory

FERMILAB-TM-2017

**Concerning Effects of Fringe Fields and Longitudinal Distribution
of b_{10} in LHC Low- β Regions**

F. Méot and A. Paris

*Fermi National Accelerator Laboratory
P.O. Box 500, Batavia, Illinois 60510*

February 1998

Disclaimer

This report was prepared as an account of work sponsored by an agency of the United States Government. Neither the United States Government nor any agency thereof, nor any of their employees, makes any warranty, expressed or implied, or assumes any legal liability or responsibility for the accuracy, completeness, or usefulness of any information, apparatus, product, or process disclosed, or represents that its use would not infringe privately owned rights. Reference herein to any specific commercial product, process, or service by trade name, trademark, manufacturer, or otherwise, does not necessarily constitute or imply its endorsement, recommendation, or favoring by the United States Government or any agency thereof. The views and opinions of authors expressed herein do not necessarily state or reflect those of the United States Government or any agency thereof.

Distribution

Approved for public release; further dissemination unlimited.

Concerning effects of fringe fields and
longitudinal distribution of b_{10}
in LHC low- β regions.

F. Méot*, A. París†

*Fermi National Accelerator Laboratory
P.O. Box 500, Batavia, Illinois 60510*

Report FERMILAB-TM-2017

February 2, 1998

Abstract

Effects of fringe fields in separation dipoles D1/D2 and low- β quadrupoles Q1-Q3 of LHC interaction regions in collision optics are investigated by means of stepwise ray-tracing in terms of aberrations, beam envelopes and other detunings. Effects of the longitudinal distribution of b_{10} error coefficient are next investigated in a similar way for assessment and comparison.

*CEA, DSM/DAPNIA/SEA, Saclay, France. fmeot@cea.fr

†University of Puerto Rico, Mayagüez.

1 Introduction

The present study aims at surveying possible effects in LHC of low- β region magnet fringe fields and longitudinal distribution of multipole errors on particle dynamics and machine parameters, in collision optics. It is performed by means of stepwise ray-tracing with the code Zgoubi. Relevant aspects of the code are made clear below (Section 2), more details can be found in Ref. [1]. A major feature of the Zgoubi integration method, of strong concern in precise and possibly multiturn tracking as involved ahead, is its ability to handle arbitrary magnetic fields with intrinsically strong symplecticity. These issues have already been subject to meticulous investigations in previous works, e.g., on the Saturne synchrotron [2] and on the LHC ring [3] ; for instance, a relevant result is the computation of the fractional tune (in a way which is discussed below) which is recovered at better than 10^{-4} in both cases, Saturne (105 m perimeter) : $\nu_x/\nu_y = 3.638574/3.620744$ from matrix transport, $\nu_x/\nu_y = 0.638564/0.620667$ from ray-tracing, and LHC (26700 m perimeter) : $\nu_x/\nu_y = 63.28000/63.31000$ from matrix transport, $\nu_x/\nu_y = 0.28006/63.31007$ from ray-tracing. Such results give confidence in the adequacy of the ray-tracing method to, on the one hand handle with precision such perturbations as end fields and other multipole defects, on the other hand provide accurate computation of machine parameters based on single- or multi-turn ray-tracing.

The present study may be considered as a continuation of earlier survey of fringe field effects in the LHC ring in injection mode optics [3]. The Version 4.2 of LHC optics is used [4]. The possible impact of fringe fields in the D1/D2 separation dipoles and in the low- β quadrupoles are investigated in terms of aberration diagrams at the interaction point (IP) (Section 3.1), beam envelopes (Section 3.2), amplitude detuning (Section 3.3) and momentum detuning (Section 3.4) effects. Similar technic is used to investigate effects of the longitudinal distribution of multipole error coefficient b_{10} (Section 4).

2 On the ray-tracing method

The Zgoubi integration method is based on stepwise resolution of Lorentz equation by a technique of Taylor series ; details can be found in Refs. [1, 3]. A major aspect relevant with the present study is the way fringe fields, multipoles and other error coefficients are simulated, this is addressed below.

2.1 Multipole magnets

The separation dipoles D1, D2 and the low- β quadrupoles can be simulated with the built-in Multipole procedure. The field and derivatives necessary for the stepwise resolution of the Lorentz equation are drawn from regular 3D scalar potential model [1, 5]

$$V_n(s, x, y) = (n!)^2 \left\{ \sum_{q=0}^{\infty} (-)^q \frac{\alpha_{n,0}^{(2q)}(s)}{4^q q! (n+q)!} (x^2 + y^2)^q \right\} \left\{ \sum_{m=0}^n \frac{\sin(m\frac{\pi}{2}) x^{n-m} y^m}{m!(n-m)!} \right\} \quad (1)$$

which in the case of the dipole and quadrupole components of concern with the low- β region magnets takes the explicit forms

$$V_1(s, x, y) = \alpha_{1,0}(s)y - \frac{\alpha_{1,0}^{(2)}(s)}{8}(x^2 + y^2)y + \frac{\alpha_{1,0}^{(4)}(s)}{192}(x^2 + y^2)^2y - \dots \quad (2)$$

$$V_2(s, x, y) = \alpha_{2,0}(s)xy - \frac{\alpha_{1,0}^{(2)}(s)}{12}(x^2 + y^2)xy + \frac{\alpha_{1,0}^{(4)}(s)}{384}(x^2 + y^2)^2xy - \dots \quad (3)$$

The s, x, y coordinates are respectively longitudinal, transverse horizontal and vertical, $\alpha_{n,0}(s)$ ($n = 1, 2, 3, \text{etc.}$) describes the longitudinal form (see Section 2.2) and $\alpha_{n,0}^{(2q)} = d^{2q}\alpha_{n,0}/ds^{2q}$ are the derivatives w.r.t. the longitudinal coordinate. Note that, in the magnet body or as well when using hard

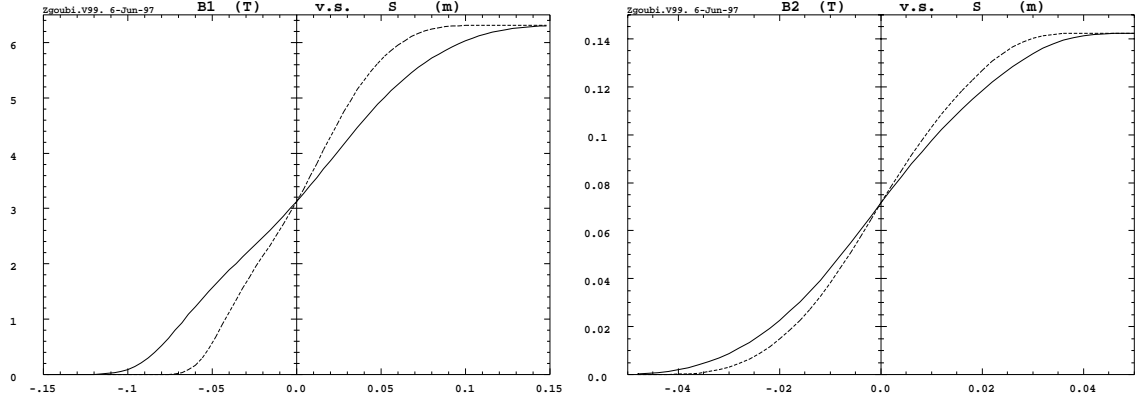


Figure 1: *Left*: field fall-off at the D1 and D2 dipole ends ; the original fall-off [7] is shown (dashed line, for $\lambda=0.056$ m), together with that used here (solid line) with Enge coefficients (Eq. 5) $\lambda=0.088$ m and $C_0 - C_5 = 0.01552, 1.93752, -0.59061, 0.37211, 0.78784, 0.46969$; the field integral relevant with matrix transport simulations is $I1 \cdot gap \approx 2.2 \cdot 10^{-2}$; the position of *EFB* is at zero, symbolized by the central vertical axis. *Right*: field fall-off at the low- β quadrupoles ; the original fall-off [8] is shown (dashed line, for $\lambda=0.056$ m), together with that used here (solid line) with Enge coefficients $\lambda=0.07$ m and $C_0 - C_5 = -0.01099, 5.46559, 0.99673, 1.55098, -5.67191, 18.57368$ ($C_0 - C_5$ values computed beforehand for $\lambda=0.056$).

edge field model, $d^{2q}\alpha_{n,0}/ds^{2q} \equiv 0$ ($\forall q \neq 0$) and hence the field and derivatives derive from the simplified potentials

$$V_1(x, y) = G_1 y, \quad V_2(x, y) = G_2 xy \quad (4)$$

where the transverse gradient G_n is constant.

Possible superimposed multipole error coefficients b_n are calculated in a similar way, this is addressed in Section 4.

2.2 Fringe field model

The field fall-off on axis at magnet ends orthogonally to the effective field boundary (*EFB*) is modeled by [6, page 240]

$$\alpha_{n,0}(d) = \frac{G_n}{1 + \exp[P(d)]}, \quad P(d) = C_0 + C_1 \frac{d}{\lambda_n} + C_2 \left(\frac{d}{\lambda_n}\right)^2 + \dots + C_5 \left(\frac{d}{\lambda_n}\right)^5 \quad (5)$$

where d is the distance to *EFB*, and the numerical coefficients $\lambda_n, C_0 - C_5$ are determined from prior matching with numerical fringe field data. This is done in such a way that $\lambda_1 \approx gap$ size in which case one can take identical $C_0 - C_5$ values whatever n while $\lambda_n \approx \lambda_1/n$; doing so λ_n can be varied at will to possibly change or test the effect of the fall-off gradient, without affecting the position of *EFB* (i.e., without any effect on the magnetic length).

The fringe fields used for D1/D2 and the low- β quadrupoles are shown in Fig. 1 which also displays the corresponding Enge coefficients, as well as the parameter $I1 \cdot gap = \int \alpha_{n,0}(s)(1 - \alpha_{n,0}(s))ds$ of concern in possible matrix transport dipole simulations. These coefficients have been obtained by a matching with, on the one hand the “White Book” data for D1/D2 [7], on the other hand Saclay data for the quadrupoles [8]. Note that these data concern the arc magnets, and have been made suitable for the present study by scaling from their actual 56 mm inner diameter to 88 mm inner diameter for the separation dipoles D1/D2 and to 70 mm inner diameter for the triplet quadrupoles.

3 Effects of fringe fields

Figure 2 obtained from MAD simulations [9, 10] shows the optical functions of the low- β region of concern in this study, namely that part of the pseudo straight section SS5 which extends between the left and right separation dipoles D1/D2. The magnets subject to fringe field effects are these separation dipoles and the low- β quadrupoles located on both sides of IP5.

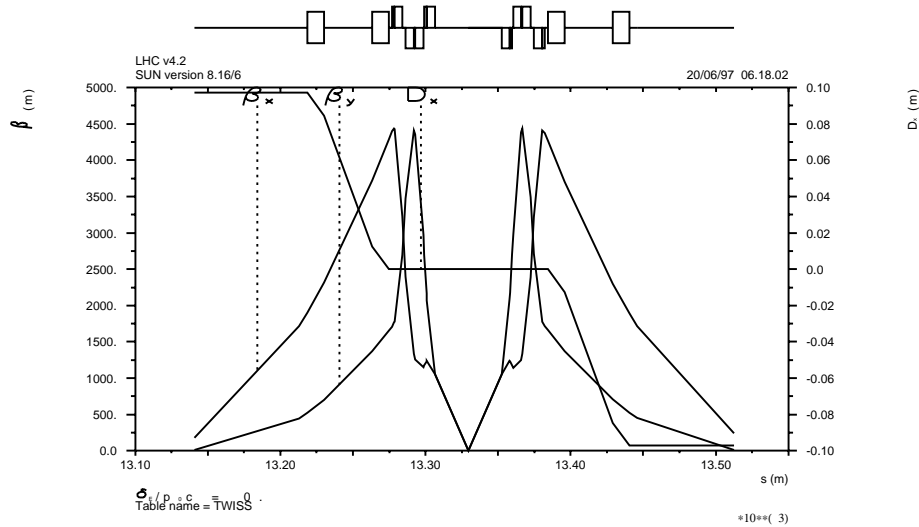


Figure 2: Optical functions across the low- β region of the interaction region IR5, in collision optics. The region of concern in this study extends from the left separation dipoles D1/D2 to their right hand side homologue, including the left and right low- β triplets.

3.1 Aberration curves at IP5

We first examine the non-linear behavior of the low- β region, in terms of the horizontal aberration curves at IP5. For this purpose we consider the piece of beam line that extends from 22.18 m upstream Q4A.L5 (222.92 m from IP5) down to IP5, in such a way as to get point-to-point imaging between the starting point (upstream end of the line) and the IP (downstream end) (Fig.3) ; point-to-point imaging allows better appreciation of distortions in transverse phase spaces under the effects of non-linearities. The first order transfer matrix of this beam line is

	x	x'	y	y'	l	dp/p
x	-0.275283	0.000000	0.000000	0.000000	0.000000	0.018782
x'	-0.023346	-3.632621	0.000000	0.000000	0.000000	0.002066
y	0.000000	0.000000	-0.224813	-8.975431	0.000000	0.000000
y'	0.000000	0.000000	-0.038357	-5.979497	0.000000	0.000000
l	-0.000158	0.068227	0.000000	0.000000	1.000000	-0.000174
dp/p	0.000000	0.000000	0.000000	0.000000	0.000000	1.000000

and has been obtained by numerical interpolation from ray-tracing of a set of paraxial rays. The coefficient value $R_{12} = 0$ ensures horizontal point-to-point imaging, which has been obtained by adjusting the initial straight section upstream Q4A.L5 to 22.18 m as mentioned above. Noting $\sigma_{x',y'} = \sqrt{\gamma_{x,y} \epsilon_{x,y} / \pi}$, $\sigma_{x,y} = \sqrt{\beta_{x,y} \epsilon_{x,y} / \pi}$, the transfer coefficients above provide the following conditions at the starting point : $\sigma_{x'} = \sigma_{x'}(IP) / R_{22} \approx -31.7 \cdot 10^{-6} / 3.633 = 8.7 \cdot 10^{-6} \text{ rad}$ and $\sigma_y = \sigma_y(IP) / R_{33} \approx -15.8 \cdot 10^{-6} / 0.225 = 70 \cdot 10^{-6} \text{ m}$.

We assess the effects of fringe fields in D1/D2 and/or the low- β quadrupoles, in presence or not of crossing at IP5. To do so, 13 particles are launched from the point object with the following coordinates :

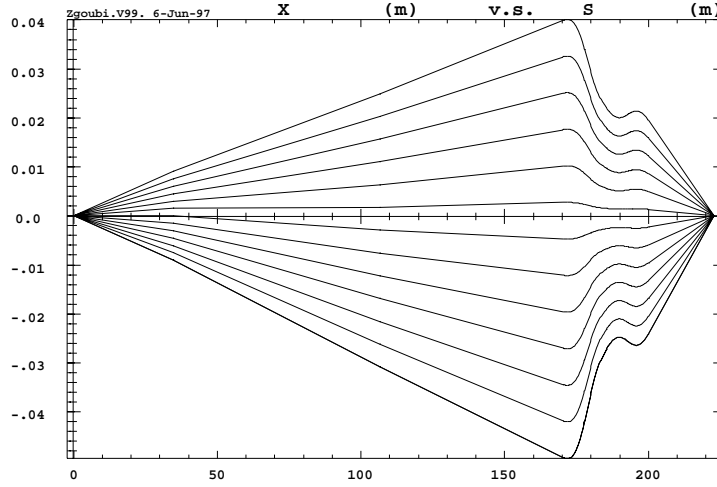


Figure 3: A set of trajectories with initial angles in the range $-30\sigma_{x'} < x'_0 < 30\sigma_{x'}$, that show the horizontal point-to-point imaging from a point source located 22.18 m upstream Q4A.L5 (222.92 m from IP5) down to IP5.

No crossing

- Fig. 4, left : $x_0 = 0$; $x'_0 = -30\sigma_{x'}$ to $30\sigma_{x'}$ step $5\sigma_{x'}$; $y_0 = 0, 5$ or $30\sigma_y$
- Fig. 4, right : $x_0 = 0$; $x'_0 = -30\sigma_{x'}$ to $30\sigma_{x'}$ step $5\sigma_{x'}$; $\delta p/p = \pm 10^{-4}$ or $\pm 10^{-3}$

Crossing

- Fig. 5, left : as Fig. 4, left
- Fig. 5, right : as Fig. 4, right

The observed aberration is of the form

$$x_{IP} \approx \left(\frac{x}{x'^3}\right)x_0'^3 \approx 5 \cdot 10^4 x_0'^3 \quad (6)$$

The first order transfer coefficient $R_{12} \equiv (x/x')$ is zero (point-to-point imaging) and leads to the aberration curve being tangent to the x' axis at the origin. The third order coefficient (x/x'^3) is mostly due to the geometrical errors introduced by the pure quadrupole fields.

A general remark as to these results is that the enlargement of the image under the effect of fringe fields is negligible, namely, whatever $|x'_0| < 30\sigma_{x'}$ one gets $\Delta x \leq \pm 10^{-6}$ m, plus possibly an additional $\pm 0.2 \cdot 10^{-6}$ due to dissymmetrization in presence of 0.1 mrad c.o. angle. Also Δy_0 vertical spread up to $30\sigma_y$ at the starting point as well as up to $10\sigma_{\delta p/p}$ momentum spread do not change the form of the aberration curve, but just move the focus point linearly in the vicinity of IP5, in proportion of the transfer coefficients above, that is to say, in a negligible way : as a consequence, the periodic motion shows negligible effect on amplitude (see next Sections).

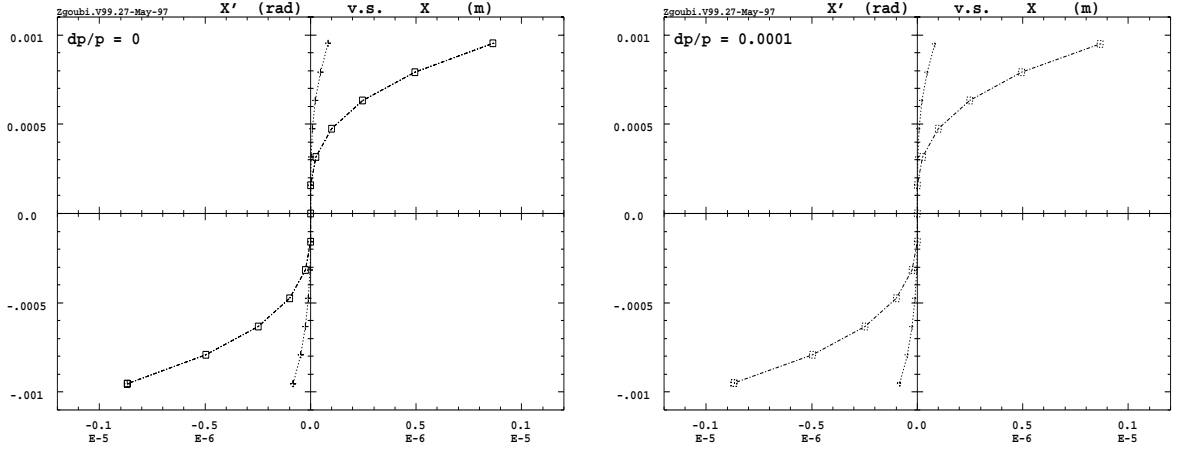


Figure 4: **Aberrations with zero closed orbit at IP5** ; the first order focusing insures that IP5 is the focus point when fringe fields are set simultaneously in the quadrupoles and in D1/D2. *Left* : a/ (squares) : fringe fields are set in quadrupoles and D1/D2 ; possible hard edge model in D1/D2 does not change the form of the aberration and just shifts the focus point by +0.03 cm w.r.t. the IP ; b/ (crosses) : fringe fields are switched off in the quadrupoles ; the focus point is shifted by -0.8 cm. Launching particles with a spread in position $y_0 = 30 \sigma_y \approx 2.116 \cdot 10^{-3}$ m (instead of $y_0 = 0$ here) makes no sensible difference apart from a spread of the focus point w.r.t. IP5. *Right* : particles are $\delta p/p = \sigma_{\delta p/p} \approx \pm 10^{-4}$ off momentum (both signs provide identical aberration curves for symmetry reasons). a/ (squares) : the focus point is shifted by ± 0.79 cm (± 0.82 cm with hard edge D1/D2) ; b/ (crosses) : the focus point is shifted by ± 0.71 cm. Launching particles with $\delta p/p = \pm 10 \sigma_{\delta p/p} \approx \pm 10^{-3}$ makes no sensible difference on the aberration curves, and results solely in linear increase in focus shift (e.g., +7.9 cm with all fringe fields on).

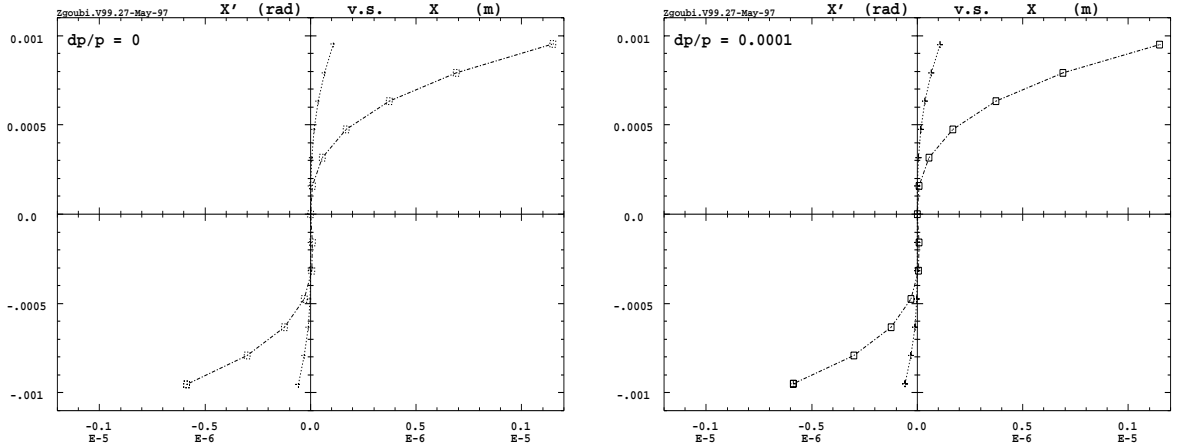


Figure 5: **Aberrations with Inclined closed orbit at IP5** ($0.1\sqrt{2}$ mrad c.o. inclined 45°). *Left* : a/ (squares) : fringe fields set in quadrupoles and in D1/D2 : the focus point is shifted by a negligible amount w.r.t. IP (and by +0.02 cm with hard edge D1/D2) ; b/ (crosses) : fringe fields are switched off in the quadrupoles (still on in D1/D2) ; the focus point is shifted by -0.8 cm. Launching particles with $y_0 = 30 \sigma_y \approx 2.116 \cdot 10^{-3}$ m makes no sensible difference. *Right* : particles are $\delta p/p = \sigma_{\delta p/p} \approx \pm 10^{-4}$ off-momentum (both signs provide identical aberration curves). a/ (squares) : the focus point is shifted by ± 0.80 cm (± 0.77 cm with hard edge D1/D2) ; b/ (crosses) : the focus point is shifted by ± 0.87 cm. Launching particles with $\delta p/p = \pm 10 \sigma_{\delta p/p} \approx \pm 10^{-3}$ makes no sensible difference on the form of the aberration curves, and entails linear increase in focus shift (e.g., ± 7.9 cm with all fringe fields on).

3.2 Periodic beam envelopes at SS5

We now adopt a different view point. We launch a single particle at IP1, on the invariants $\sigma(\epsilon_{x,y}/\pi)$ or $900 \sigma(\epsilon_{x,y}/\pi)$ (i.e., $30 \sigma_{x,y}$) for a 100-turn tracking including stepwise ray-tracing through all optical elements in the range Q4A.L5/VK2.R5¹ (Fig. 2) as in the previous sections while the rest of the machine is represented by first order matrix transfer ; this first order mapping has been obtained from preliminary MAD simulations, in particular transfer coefficients with high enough accuracy to ensure good symplecticity have been computed from a MAD-SURVEY output file by means of a postprocessor based on the computer code RDTWISS [13].

Our goal is to generate beam envelopes and survey possible alteration of their sizes upon effects of fringe fields. Considering their weakness as revealed in the previous Sections we limit the investigation to the case of inclined $0.1\sqrt{2}$ mrad c.o. angle to allow for extreme transverse excursion of the particles in the low- β quadrupoles. For reference, the following figures are expected in one or the other transverse plane :

- maximum amplitude, in case of no crossing angle :
 $\max(x,y) = \sqrt{\beta\epsilon/\pi} = 1.49 \cdot 10^{-3}$ m for the one- σ envelope and $4.46 \cdot 10^{-2}$ m for 30σ
in the low- β regions (i.e., inside quadrupoles Q2 or Q3 where β reaches 4400 m),

- maximum amplitude with 0.1 mrad projected c.o. angle at IP5 :
 $\max(x,y) = 4.7 \cdot 10^{-3} + \sqrt{\beta\epsilon/\pi} = 6.19 \cdot 10^{-3}$ m for the one- σ envelope and $4.93 \cdot 10^{-2}$ m for 30σ .

Exact values are displayed at the foot of Figs. (6) and appear to depart in a negligible way from the preceding ones. A general comment on these plots is that up to the explored value $\sigma_0 = 30 \sqrt{\beta\epsilon/\pi}$, no non-linear envelope variation $\frac{\Delta\sigma}{\sigma_0}$ can be observed in either plane. This shows the weakness of the effects of fringe fields on beam envelopes.

¹The vertical crossing angle bump [11] is closed with an *ad hoc* dipole “VK2.R5” located right upstream Q4A.R5 [12] ; otherwise specified, elements are named after the LHC Version 4.2 nomenclature [9, 10].

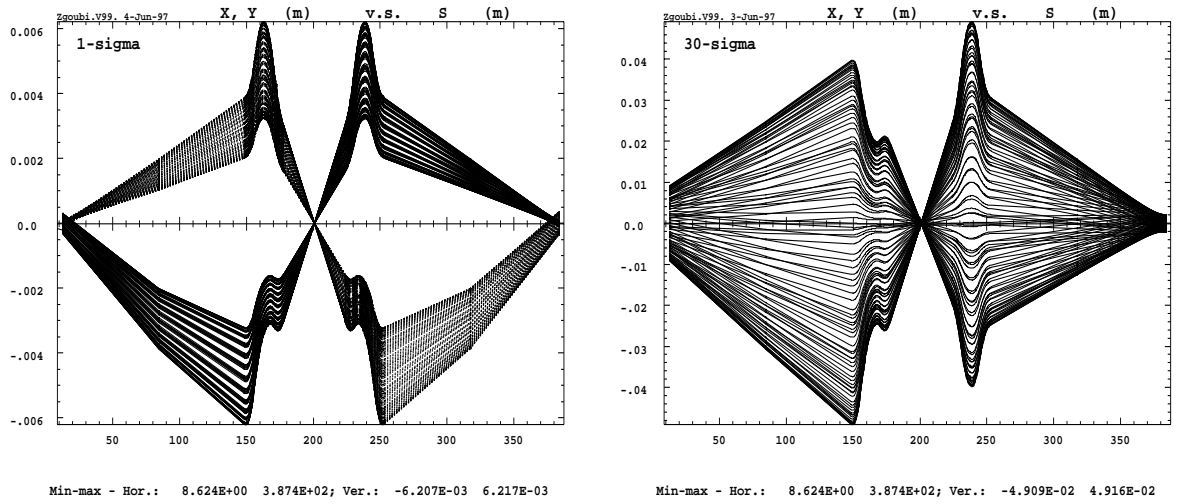


Figure 6: Beam envelopes at SS5. The closed orbit angle at IP5 is 0.1 mrad in the horizontal plane and -0.1 mrad in the vertical plane ; fringe field model is set in all magnets. *Left* : projection of the $\sigma_{x,y}$ periodic beam envelope ($\epsilon_{x,y}/\pi = 5 \cdot 10^{-10}$ m.rad) onto the horizontal plane (solid lines) and onto the vertical plane (dashed lines) (Note that, due to the antisymmetry of the triplet optics this plot can also be viewed as the projection of the intersection of beam 1 and beam 2). *Right* : projection of the $30 \sigma_{x,y}$ periodic beam envelope ($\epsilon_{x,y}/\pi = 4.5 \cdot 10^{-7}$ m.rad) onto the horizontal plane ; no sensible effect of the non-linearities is observed : the beam envelope varies in proportion of the square root of the invariant from the left plot to the right one ; similar behavior is obtained for the unshown vertical envelope.

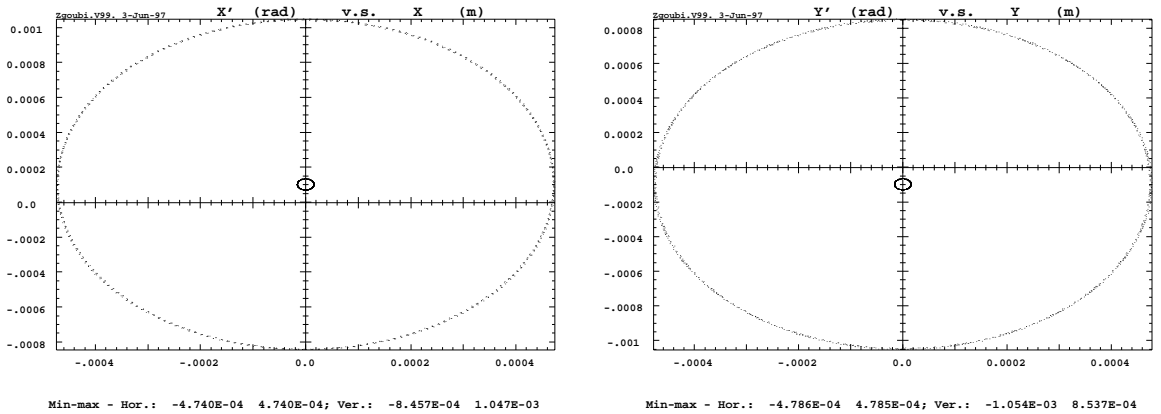


Figure 7: Horizontal (left) and vertical (right) 600-turn phase space ellipses at IP5, in the same conditions as above. The small ellipse is for a particle launched on the one-sigma invariants ($\epsilon_{x,y}/\pi = 5 \cdot 10^{-10}$ m.rad), the large ellipse is for $30 \sigma_{x,y}$ ($\epsilon_{x,y}/\pi = 4.5 \cdot 10^{-7}$ m.rad). The horizontal phase space (left figure) is centered on $x'^* = 0.1$ mrad c.o. angle at IP5, while the vertical phase space (right figure) is centered on $y'^* = -0.1$ mrad c.o.

3.3 Amplitude detuning

Tunes vs. amplitude are computed by means of 1000-turn ray-tracing of particles launched at IP1 with zero angle and up to $30\sigma_{x,y} = 0.475 \cdot 10^{-3}$ m amplitude in both planes. Here again ray-tracing is performed only within the range Q4A.L5/VK2.R5 ; beyond this range first order matrix transport is used. The phase space coordinates are observed at the IP.

3.3.1 Hard edge magnets, no crossing at IP5

Ray-tracing in hard edge magnets without crossing is first performed in order to show that the first order machine parameters are accurately recovered, in conformity with MAD simulations. Tune values vs. amplitude are reported in Table 1. On the other hand, these preliminary results are intended as a basis for consistent comparison with further ray-tracing including fringe fields and/or crossing angle(s).

3.3.2 Magnets with fringe fields, and crossing at IP5

An horizontal closed orbit angle $x'_{co} = 10^{-4}$ rad is first introduced at IP5 following regular orbit geometry and including compensation of the anomalous dispersion due to crossing by pairs of quadrupoles placed at IR ends [12]. Except otherwise quoted the invariant smear does not exceed 10^{-3} . Figure 8 displays a specimen of the phase space trajectories (here, observed at IP1), as used for Fourier analysis from which Table 2 derives.

Fringe fields in low- β quadrupoles only are first set and lead to the amplitude detuning listed in the third column of Table 2. Fringe fields are next simultaneously set in the dipoles D1/D2 and in the low- β quadrupoles which leads to the fourth column of Table 2.

Finally, $0.1\sqrt{2}$ mrad inclined c.o. angle at IP5 is set together with all fringe fields ; this leads to the amplitude detuning values shown in the fifth column of Table 2. It can be observed that the tune footprint is very small : less than 10^{-4} for both horizontal and vertical motions at $10\text{-}\sigma_{x,y}$ amplitude, less than $8 \cdot 10^{-4}$ at $30\text{-}\sigma_{x,y}$.

3.4 Momentum detuning

We now launch particles with amplitudes ranging from 10^{-2} to $30\sigma_{x,y}$ as in the previous section, but with in addition momentum deviation $\delta p/p = \pm 10^{-5}$ and $\delta p/p = \pm 6 \cdot 10^{-4} \approx 5 \sigma_{\delta p/p}$. Results are gathered in Table 3. From comparison with Table 2 the chromaticities come out to be $\delta\nu_x/\delta p/p = \delta\nu_y/\delta p/p \approx -30$ whatever $\delta p/p$ (this is about the contribution of an IR to the chromaticity in collision optics with $\beta^* = 0.5$ m [4]). This makes clear that fringe fields do not introduce sensible non-linear chromatic effects.

Table 1: Tune values as a function of x, y amplitudes obtained with hard edge magnets, from one thousand turns Fourier analysis. The symplecticity is controlled in terms of the smear of the invariant, and shows to behave well enough (less than $6 \cdot 10^{-3}$ smear is observed, and no spiraling effect). This Table is mostly intended to show that ray-tracing reproduces the quasi independence of tunes on amplitude as expected in the linear approximation, and to serve as a basis for further comparisons.

x_0/σ_{x_0}	y_0/σ_{y_0}	ν_x/ν_y
10^{-2}	10^{-2}	0.280013 / 0.309735
10		0.280016 / 0.309737
20		0.280026 / 0.309740
30		0.280044 / 0.309746
10^{-2}	10	0.280014 / 0.309739
10		0.280018 / 0.309740
20		0.280028 / 0.309743
30		0.280045 / 0.309749
10^{-2}	20	0.280018 / 0.309748
10		0.280021 / 0.309749
20		0.280032 / 0.309753
30		0.280049 / 0.309759
10^{-2}	30	0.280024 / 0.309763
10		0.280028 / 0.309765
20		0.280038 / 0.309768
30		0.280056 / 0.309774

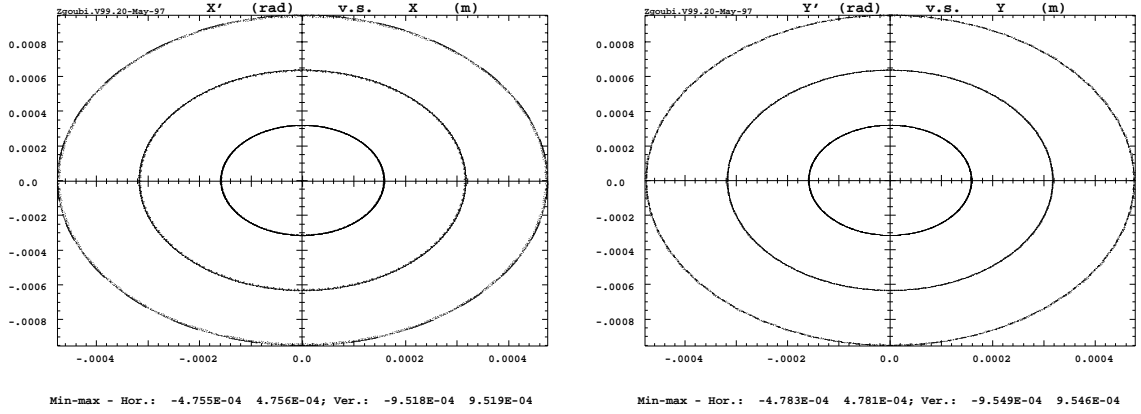


Figure 8: A specimen of 10^3 -turn horizontal and vertical phase space plots as observed at IP1, and used for determining the tune values displayed in Table 2. Conditions set at IP5 are, in the present case, fringe fields in D1/D2 and in the low- β quadrupoles and horizontal c.o. angle $x'^* = 10^{-4}$ rad - the vertical c.o. is zero. The horizontal and vertical invariants range from zero to $900 \sigma(\epsilon_{x,y}/\pi)$ (i.e., $30 \sigma_{x,y}$). The thickness of the presumably invariant ellipse is due mostly to the non-zero motion in the orthogonal plane, however the smear of the invariant does not exceed $6 \cdot 10^{-3}$ (except for very small amplitude motions where coupling can arise from either kinematic effects or field terms of order two and higher in x, y). This confirms the correct symplecticity of the ray-tracing and the validity of its outcomes in this respect.

Table 2: Tune values vs. amplitude. *First two columns* : initial horizontal and vertical sampling, in units of $\sigma = \sqrt{\beta\epsilon/\pi}$, from 10^{-2} to 30σ ; *third column* : fringe fields at IP5 in low- β quadrupoles only (D1/D2 are hard edge) with horizontal c.o. angle $x'_{co} = 10^{-4}$ rad and zero vertical c.o. at IP5. *fourth column* : fringe fields in dipoles D1/D2 and low- β quadrupoles, with horizontal c.o. angle $x'_{co} = 10^{-4}$ rad and zero vertical c.o.. *fifth column* : fringe fields in dipoles D1/D2 and low- β quadrupoles at IP5, with horizontal and vertical c.o. angle $x'_{co} = -y'_{co} = 10^{-4}$ rad at IP5. The last two lines give the footprint size in the tune diagram for respectively $10\sigma_{x,y}$ and $30\sigma_{x,y}$ amplitude motion.

x_0/σ_{x_0}	y_0/σ_{y_0}	ν_x/ν_y		
		Fringe field in quads	Fringe field in quads and D1/D2	All fringe fields and inclined Xing
10^{-2}	10^{-2}	0.279717 / 0.309431	0.279781 / 0.309629	0.279791 / 0.309642
10		0.279748 / 0.309486	0.279815 / 0.309683	0.279827 / 0.309702
20		0.279853 / 0.309628	0.279920 / 0.309829	0.279929 / 0.279931
30		0.280015 / 0.309876	0.280088 / 0.310077	0.280099 / 0.280103
10^{-2}	10	0.279764 / 0.309469	0.279835 / 0.309665	0.279850 / 0.309680
10		0.279797 / 0.309518	0.279870 / 0.309719	0.279880 / 0.309732
20		0.279903 / 0.309663	0.279966 / 0.309861	0.279976 / 0.309875
30		0.280069 / 0.309913	0.280138 / 0.310110	0.280147 / 0.310124
10^{-2}	20	0.279920 / 0.309565	0.279980 / 0.309767	0.279995 / 0.309780
10		0.279950 / 0.309612	0.280014 / 0.309813	0.280024 / 0.309826
20		0.280049 / 0.309766	0.280121 / 0.309968	0.280130 / 0.309981
30		0.280214 / 0.310013	0.280281 / 0.310215	0.280292 / 0.310228
10^{-2}	30	0.380536 / 0.309735	0.280235 / 0.309935	0.280243 / 0.309949
10		0.280199 / 0.309782	0.280263 / 0.309985	0.280274 / 0.309998
20		0.280299 / 0.309932	0.280369 / 0.310129	0.280378 / 0.310144
30		0.280462 / 0.310180	0.280532 / 0.310377	0.280543 / 0.310393
Tune footprint size				
for $10\sigma_{x,y}$.8 10^{-4} / .9 10^{-4}	.9 10^{-4} / .9 10^{-4}	.9 10^{-4} / .9 10^{-4}
for $30\sigma_{x,y}$		7.5 10^{-4} / 7.5 10^{-4}	7.5 10^{-4} / 7.5 10^{-4}	7.5 10^{-4} / 7.5 10^{-4}

Table 3: Tune values vs. momentum and amplitude. All fringe fields are set, inclined c.o. angle.

x_0/σ_{x_0}	y_0/σ_{y_0}	ν_x/ν_y			
		$\delta p/p = -6 \cdot 10^{-4}$	$\delta p/p = -10^{-5}$	$\delta p/p = 10^{-5}$	$\delta p/p = 6 \cdot 10^{-4}$
10^{-2}	10^{-2}	0.297700 / 0.327696	0.280091 / 0.309942	0.279499 / 0.309351	0.262335 / 0.292436
10		0.297733 / 0.327745	0.280125 / 0.280119	0.279531 / 0.309402	0.262369 / 0.292487
20		0.297823 / 0.327891	0.280219 / 0.280221	0.279638 / 0.309551	0.262483 / 0.292647
30		0.297987 / 0.328132	0.280390 / 0.280393	0.279798 / 0.279805	0.262658 / 0.292906
10^{-2}	10	0.297753 / 0.327727	0.280145 / 0.309976	0.279551 / 0.309383	0.262388 / 0.292469
10		0.297779 / 0.327780	0.280172 / 0.310023	0.279582 / 0.309436	0.262423 / 0.292526
20		0.297869 / 0.327922	0.280268 / 0.310174	0.279686 / 0.309584	0.262535 / 0.292679
30		0.298032 / 0.328162	0.280437 / 0.310422	0.279853 / 0.309831	0.262715 / 0.292939
10^{-2}	20	0.297891 / 0.327832	0.280290 / 0.310070	0.279705 / 0.309490	0.262553 / 0.292580
10		0.297921 / 0.327878	0.280323 / 0.310120	0.279732 / 0.309538	0.262582 / 0.292629
20		0.298019 / 0.328025	0.280420 / 0.310270	0.279833 / 0.309687	0.262693 / 0.292788
30	0	0.298176 / 0.328266	0.280591 / 0.310517	0.279997 / 0.309936	0.262865 / 0.293049
10^{-2}	30	0.298136 / 0.327993	0.280543 / 0.310240	0.279953 / 0.309650	0.262816 / 0.292747
10		0.298162 / 0.328046	0.280574 / 0.310286	0.279981 / 0.309705	0.262844 / 0.292804
20		0.298257 / 0.328183	0.280669 / 0.310440	0.280085 / 0.309848	0.262957 / 0.292954
30		0.298416 / 0.328425	0.280838 / 0.310687	0.280245 / 0.310096	0.263129 / 0.293215

4 Effect of longitudinal distribution of b_{10} in quadrupoles

The multipole error coefficients in the low- β quadrupoles are simulated from the general scalar potential (Eq. 1). The particular form it takes for b_{10} component is,

$$V_{10}(s, x, y) \approx \left\{ \alpha_{10,0} - \frac{\alpha''_{10,0}}{44} (x^2 + y^2) \right\} \{ 10x^8 - 120x^6y^2 + 252x^4y^4 - 120x^2y^6 + 10y^8 \} \quad (7)$$

Our goal is twofold : on the one hand assess the importance of the way b_{10} is distributed along the quadrupole, on the other hand establish a concordance with anterior results in which b_{10} is proved to have a determinant effect on dynamic aperture (DA) [14, 15]. In the simulations that follow we investigate three models (Fig. 9) : either hard edge, or a regular smooth fall-off at quadrupole ends (Eq. 5), or a lump model in which b_{10} is zero in the body and the integral strength is shared between the two ends (after Ref. [16]).

For simplification b_{10} is set in all quadrupoles, or at all quadrupole ends in the case of the lump model, regardless of their respective influence which is in fact highly correlated to the magnet position because of the strong dependence of the effects on the betatron function².

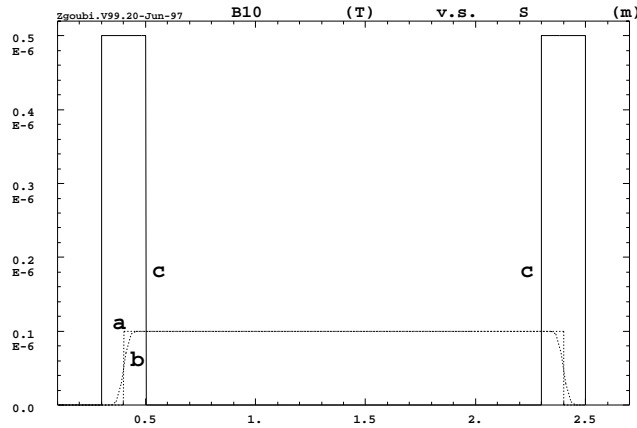


Figure 9: Fringe field models used for assessing the effect of b_{10} error multipole on particle dynamics : (a) hard edge, (b) fringe field fall-off, (c) lump distribution at EFB's. In all three cases the overall field integral is the same and $b_{10} = -0.005 (10^{-4})$ is assumed [14].

4.1 Aberration curves at IP5

It can be seen from Fig. 10 that $b_{10} = -0.005 10^{-4}$ strongly distorts the aberration curves originally shaped as in Figs. (4, 5). The aberration is of the form

$$x_{IP} \approx \left(\frac{x}{x'^3} \right) x_0'^3 + \left(\frac{x}{x'^9} \right) x_0'^9 \quad (8)$$

where x_0' is the starting angle (Fig. 3) ; this is to be compared to anterior work on the calculation of aberration coefficients in the low- β regions [17]. The first order transfer coefficient (x/x') is zero (point-to-point imaging as schemed in Fig. 3), the third order coefficient (x/x'^3) is mostly due to the geometrical errors introduced by the quadrupole and has the same value as in Section 3.1 (Eq. 6)

²Tracking shows for instance that only a very strong change of b_{10} in Q1.Left or Q1.Right will change the DA.

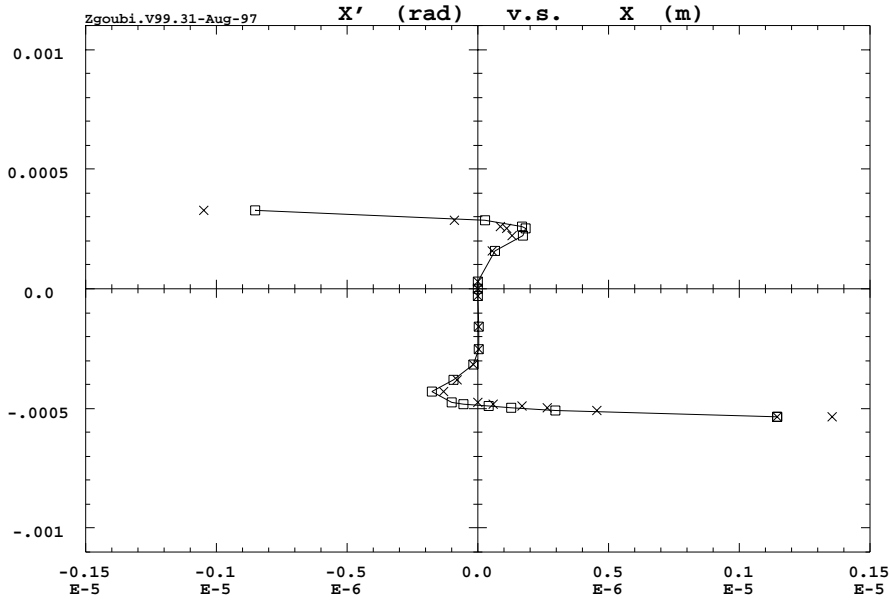


Figure 10: **Aberrations with inclined closed orbit at IP5** ($0.1\sqrt{2}$ mrad c.o. angle at 45°) ; fringe fields are set in D1/D2 and in the quadrupoles for the main component b_2 . *Squares* : aberration curve obtained with either hard edge or fringe field model for b_{10} : practically no difference can be observed between the two at that scale and in this range of initial angles. *Crosses* : aberration curve obtained with lump b_{10} model : the difference with the previous case is weak, mostly the turn-round occurs at slightly lower x' value (presumably detrimental to the dynamic aperture), and the curve stretches a little bit more. The dramatic effect of b_{10} can be checked by comparison with Figs. 4, 5 : one can see that the $\pm 1\mu\text{m}$ excursion is reached within much smaller acceptance in presence of b_{10} , namely with $|x'_0| < 10\sigma_{x'_0}$ instead of $|x'_0| < 30\sigma_{x'_0}$ if b_{10} is off.

and the ninth order coefficient (x/x'^9) is due to b_{10} . (x/x'^3) and (x/x'^9) have opposite signs and therefore act in opposite ways, resulting in the turn-round region between the two effects (Fig. 10), which gets closer to the x-axis the stronger b_{10} . In particular with the present value $b_{10} = -5 \cdot 10^{-3}$ (10^{-4}) a $\pm 1 \mu\text{m}$ extent at the image is reached with starting angle $\approx -10 \sigma_{x'_0}$ or $+15 \sigma_{x'_0}$, about twice smaller than without b_{10} (Figs. 4, 5).

4.2 DA tracking

Multiturn tracking is performed in order to assess the effect of b_{10} model on the dynamic aperture. At first sight, considering the violent turn-round in the aberration curves (Fig. 10) and the fact that it occurs at $x'_0 \approx 10 \sigma_{x'}$ whatever the longitudinal model for b_{10} , it can be expected that, on the one hand all three models provide similar DA, on the other hand the DA be about 10σ as well.

This is confirmed in Table 4 in which DA tracking results are gathered, and, as to the hard edge model, is in agreement with results published elsewhere [14, 15]. Fig. (11) provides a sample of transverse phase space at the stability limit.

Table 4 also displays DA tracking results in presence of defects in both IP1 and IP5 low- β regions with various crossing signs, which show that interference effects between the two may slightly change the DA.

Table 4: 1000-turn DA values for the three b_{10} models. Test particles have either zero y motion ($y=0$), or identical initial x and y coordinates ($x=y$) or zero x motion ($x=0$). Defects are set either only at IP5 (cols. 2, 3) or at IP1 and IP5 simultaneously (cols. 4, 5). Crossings are either inclined (cols. 2, 4) or in the horizontal plane (cols. 3, 5). The scan resolution is $\pm 0.1 \sigma_{x,y}$

Field model	Dynamic aperture (units of σ)			
	single IP		IP1 and IP5	
	inclined 0.28 mrad $y=0/x=y/x=0$	horizontal 0.2 mrad $y=0/x=y/x=0$	inclined 0.28 mrad -- / + + ^a $y=0/x=y/x=0$	inclined 0.28 mrad + + / + + ^b $y=0/x=y/x=0$
Hard edge	13.1/9.7/12.9	13.0/10.9/16.1	12.3/9.8 /12.8	12.8/9.6/11.3
Fringe field	13.0/9.7/12.9	13.1/11.1/16.0	12.2/10.3/12.8	12.8/9.6/11.3
Lump at EFB	13.1/9.8/12.9	13.1/11.1/16.4	11.9/10.0/13.0	13.0/9.8/11.3 ^c

^a c.o. angles are $x'_{IP1} = -0.1$ mrad, $y'_{IP1} = -0.1$ mrad, $x'_{IP5} = 0.1$ mrad, $y'_{IP5} = 0.1$ mrad,

^b c.o. angles are $x'_{IP1} = 0.1$ mrad, $y'_{IP1} = 0.1$ mrad, $x'_{IP5} = 0.1$ mrad, $y'_{IP5} = 0.1$ mrad,

^c Phase space plot is shown in Fig. 11

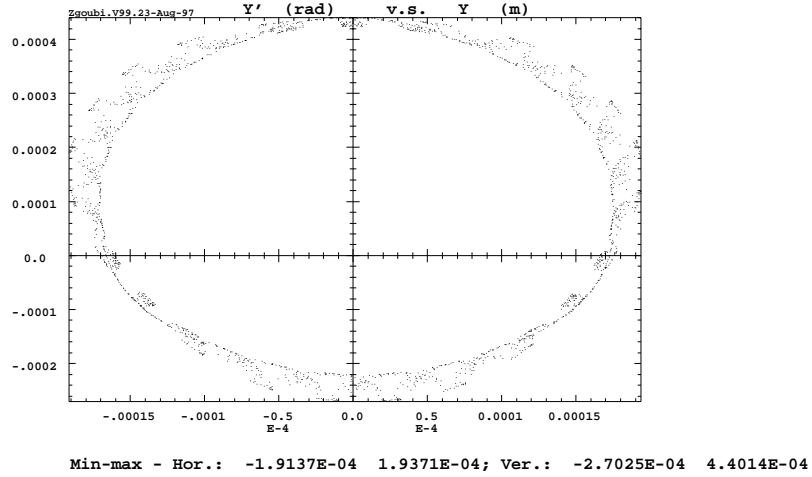


Figure 11: A sample of vertical phase space plot at the stability limit : particle launched with $x=x'=y=0$ and $y' = 11.0 \sigma$, in presence of inclined 0.14 mrad c.o. angles of identical signs at IP1 and IP5 simultaneously, with lumped b_{10} model (longitudinal distribution 'c' in Fig. 9).

Table 5: Amplitude detuning in presence of b_{10} error. *First column* : initial amplitude on the diagonal ($x=y$) in units of $\sigma = \sqrt{\beta\epsilon/\pi}$, from 10^{-2} to the DA limit ; *third to fourth columns* : three cases of longitudinal model for b_{10} as schemed in Fig. (9). The last line gives the footprint size in the tune diagram for motion amplitude up to the DA.

$\frac{x_0}{\sigma_{x_0}} = \frac{y_0}{\sigma_{y_0}}$	ν_x/ν_y		
	Hard edge	Fringe field	Lump
10^{-2}	0.280014 / 0.309737	0.279726 / 0.309447	0.279726 / 0.309447
5	0.279978 / 0.309700	0.279710 / 0.309425	0.279719 / 0.309431
9.3	0.279392 / 0.309811	0.279137 / 0.309581	0.279359 / 0.309516
9.7	0.279176 / 0.310273	0.278938 / 0.309895	
9.8			0.279157 / 0.309793
Footprint size	$8.4 \cdot 10^{-4} / 5.4 \cdot 10^{-4}$	$7.9 \cdot 10^{-4} / 4.5 \cdot 10^{-4}$	$5.7 \cdot 10^{-4} / 3.3 \cdot 10^{-4}$

4.3 Amplitude detuning

The following Table 5 shows that the tune footprints are also enlarged under the effect of b_{10} , compared to what they were without b_{10} (cf. last lines in Table 2). They remain however small enough that the DA so calculated be attributed to the geometrical aberrations - not to detuning effects.

5 Conclusions

Effects of low- β region fringe fields on LHC parameters in collision optics ($\beta^* = 0.5$ m and $0.1\sqrt{2}$ mrad inclined c.o. angle) have been studied in detail. It has been shown that they are innocuous up to invariant values far beyond machine acceptance. In particular, in presence of fringe fields the tune footprint remains smaller than 10^{-4} within $10\sigma_{x,y}$ amplitude, and no additional non-linear chromatic effects can be observed within $5\sigma_{\delta p/p}$ momentum dispersion range.

Similar study has been performed with systematic error coefficient $b_{10} = -0.005 \cdot 10^{-4}$. Its bare effect as assessed in Ref. [14] (about 10σ DA, diagonal) has been confirmed ; it has been shown that the form of its longitudinal distribution has negligible impact on the DA, by investigating various extreme models which affect its value by no more than about 5%.

This work has strongly benefited from discussions within the LHCAP Group meetings at FER-MILAB, and with A. Verdier and J.-P. Koutchouk who further read the manuscript.

References

- [1] F. Méot and S. Valéro, Zgoubi users' guide, Note CEA/DSM/LNS/GECA/97-43 and FERMILAB-TM-2010, FNAL, 1997.
- [2] F. Méot, A numerical method for the ray-tracing of polarized beams, Proc. EPAC Conf., 1992.
- [3] F. Méot, On the effects of fringe fields in the LHC ring, Part. acc., 1996, Vol. 55, pp.[329-338]/83-92.
- [4] The Large Hadron Collider, Conceptual Design, CERN/AC/95-05 (LHC), CERN, 20 Oct. 1995.
- [5] G. Leleux, Compléments sur la physique des accélérateurs, DEA de Physique et Technologie des Grands Instruments, rapport CEA/DSM/LNS/86-101, CEA, Saclay (1986).
- [6] H.A. Enge, Deflecting magnets, in *Focusing of charged particles*, volume 2, A. Septier ed., Academic Press, New-York and London (1967).
- [7] The Large Hadron Collider Accelerator Project, LHC CERN AC/93-03 ; the magnetic field data have been provided by S. Russenchuck, CERN/AT/MA (1994).
- [8] Saclay data for arc quadrupoles are used, they have been provided by S. Russenchuck, CERN/AT/MA (1994).
- [9] H. Grote, F. C. Iselin, The MAD Program, User's Reference Manual, CERN/SL/90-13 (AP), CERN, 19 Jan. 1995.
- [10] T. Risselada, CERN/SL/AP, provided the MAD files lhc42.K-collision, lhc42.K-injection, lhc42.sequence, for LHC Version 4.2 optics.
- [11] J. Miles, in Proc. LHC Machine Advisory Committee, CERN, Nov. 6, 1996.
- [12] F. Méot, Crossing Angle Induced Dispersion in LHC, FERMILAB-TM-2001, May 1997.
- [13] J. Jowett, RDTWISS computer code, private communication, CERN, 1994.
- [14] A. Faus-Golfe and A. Verdier, Dynamic aperture limitations of the LHC in physics conditions due to low- β insertions, Proc. EPAC Conf. 1996.
- [15] W. Chou, private communication, tracking results with JJIP, FNAL, 1997, and W. Chou, D. Ritson, Dynamic aperture studies during collisions in the LHC, CERN/LHC Project Report 123, Proc. PAC Conf. 1997.
- [16] S. Caspi and K. Chow, Normal and skew multipoles in the LHC low- β quad. - Rev. 1., SC-MAG-577, LBNL, Berkeley, CA, Feb. 1997.
- [17] A. Faus-Golfe and A. Verdier, Multipole compensation in the LHC low- β insertions, LHC Project Report 116, CERN, 9 June 1997 ; Proc. PAC Conf., Vancouver, 1997.